Spectrochimica Acta Part A: Molecular and Biomolecular Spectroscopy 268 (2022) 120647

Contents lists available at ScienceDirect

Spectrochimica Acta Part A: Molecular and Biomolecular Spectroscopy

journal homepage: www.elsevier.com/locate/saa

Temperature-sensitive emission of dialkylaminostyrylhetarene dyes and their incorporation into phospholipid aggregates: Applicability for thermal sensing and cellular uptake behavior

B.S. Akhmadeev [a,*], T.P. Gerasimova [a], A.R. Gilfanova [a], S.A. Katsyuba [a], L.N. Islamova [a], G.M. Fazleeva [a], A.A. Kalinin [a], A.G. Daminova [b], S.V. Fedosimova [b], S.K. Amerhanova [a], A.D. Voloshina [a], E.G. Tanysheva [a], O.G. Sinyashin [a], A.R. Mustafina [a]

[a] Arbuzov Institute of Organic and Physical Chemistry, FRC Kazan Scientific Center of RAS, 8 Arbuzov st., 420088 Kazan, Russian Federation
[b] Kazan (Volga region) Federal University, 18 Kremlyovskaya st., 420008 Kazan, Russian Federation

HIGHLIGHTS

- Push-pull dyes are temperature-sensitive luminophores in dichloromethane solutions.
- Hydrophobicity-driven incorporation of the dyes into phospholipid-based bilayers.
- Temperature sensitive emission of the dyes within phospholipid-bilayers.
- Optimal dye for high temperature sensitivity and reversibility under heating/cooling.
- The dye within bilayers efficiently stains the cell cytoplasm with low cytotoxicity.

GRAPHICAL ABSTRACT

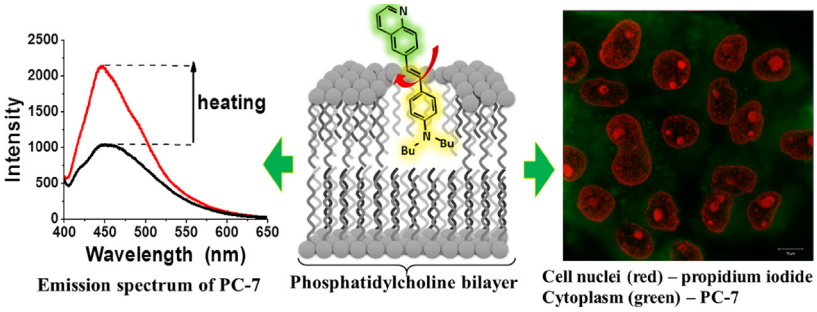

ARTICLE INFO

Article history:
Received 18 September 2021
Received in revised form 25 October 2021
Accepted 16 November 2021
Available online 19 November 2021

Keywords:
Dye
Structure–property relationship
Phospholipid bilayer
Cellular marking
Temperature sensitive luminescence

ABSTRACT

A series of dialkylaminostyrylhetarene dyes constructed from electron-rich and electron-deficient moieties of various structures connected *via* vinylene π-bridges are introduced as temperature-sensitive luminophores. The temperature dependent emission of the dyes in the acidified dichloromethane solutions derives from temperature-induced shift of the equilibrium between neutral and protonated forms of the dyes. The heating-induced blue shift and intensification of emission of neutral form of the dyes make them a promising basis for development of nanoparticles exhibiting temperature-sensitivity in aqueous solutions at pH typical of biological liquids. Hydrophobicity-driven incorporation of the water insoluble dyes into L-α-phosphatidylcholine(PC)-based bilayers allows to obtain water dispersible dye-PC aggregates, and to follow their emission in the aqueous solutions. Structure of the dyes has strong impact on the efficacy of the dyes incorporation into the PC-based bilayers, temperature sensitivity of emission of the dye-PC aggregates and its reversibility under the heating/cooling cycles. This enables structural optimization of the dyes in order to obtain the dye-PC species demonstrating maximal temperature dependence and reversibility of their luminescence in aqueous solutions. The selected leader exhibits low cytotoxicity exemplified for M–HeLa and Chang Liver cell lines, while the efficient cell internalization of the dye, manifested in the staining of the cell cytoplasm, opens further opportunities for biosensing applications.

* Corresponding author.
E-mail address: bulat_ahmadeev@mail.ru (B.S. Akhmadeev).

https://doi.org/10.1016/j.saa.2021.120647
1386-1425/

1. Introduction

Structure-property relationships for organic dyes encapsulated into phospholipid bilayers have gained great interest due to their impact on developing of various sensing techniques [1–10]. The role of phospholipid (PhL) bilayers as nanobeads for dye molecules is to enhance their water solubility and biocompatibility. In turn, the well-known sensitivity of the dyes emission to any changes in their microenvironment and versatility of their spectral properties provide a basis for applications in sensing of the temperature-induced phase transitions of PhL bilayers resulted from the changes from an order to fluidity [1–10]. Moreover, efficient cell internalization of dye-PhL vesicles through the endocytic pathway is the already documented basis for their acting as vehicles for the cytoplasmatic delivery of dyes into cells [11–13]. The cell internalization of the dye, in turn, opens an opportunity to utilize it for sensing of biorelevant intracellular processes, including intracellular trafficking of drugs, exocytosis, membrane composition [14–20].

Monitoring of local heating in the intracellular space is of great impact in anticancer therapy [21,22,23], which prompts developing of specific nanoarchitectures combining therapy and sensing functions. The already documented abilities of PhL bilayers to be deposited onto nanoparticles [24] or to serve as nanobeads for amphiphilic molecules [25] makes mixed dye-PhL bilayers a promising basis for combining sensing and therapy functions in one nanoparticle.

The formation of mixed dye-PhL aggregates is driven by both electrostatic and Van der Waals interactions. The mutual balance of the aforesaid interactions can be tuned by the structure variation of the dyes. Thus, development of dye-PhL bilayers with temperature-sensitive spectral properties should begin with optimization of the dye structure, which must be suitable both for efficient embedding into the PhL bilayer and for producing spectral response to temperature changes. The quinoxalinone based push–pull luminophores [26] constructed from electron-rich and electron-deficient moieties connected via vinylene-bridges (Scheme 1) exhibit the charge distribution highly sensitive to such external stimuli as electric field variation or interactions with molecular dipoles and ions. This sensitivity results in nonlinear optical activity [27,28] or solvatochromic and halochromic properties of such dyes [29]. Moreover, these species have already demonstrated the ability to form mixed dye-PhL bilayers, which show spectral response to the pH change in water caused by the protonation of the dyes [29]. Thus, both the specific structure of the dyes and their previously reported solvatochromic and halochromic properties [29] suggest a possibility of thermo-sensitive fluorescence of the mixed dye-PhL bilayers caused by a temperature shift of the acid/base equilibrium of the dye and/or temperature-induced dislocation of dye molecules within the bilayer zones with different polarity [3–6]. The aim of the present work is (1) to find the optimal dye structure for creating mixed dye-PhL aggregates with high thermal sensitivity, low cytotoxicity, and high cell internalization, and (2) to identify the main reasons for the thermal-sensitive fluorescence of mixed dye-PhL bilayers.

The dyes **1** and **3** with 6th position of donor dialkylaniline moiety were shown [29] to provide the best combination of the brightest luminescence and maximal halochromism within the series and good compatibility with PhL. In present study we broaden structural variation of dyes via replacement of quinoxalinone moiety in molecules **1** and **3** with three different heterocyclic substituents (**6**, **7** and **8**). The choice of phosphatidylcholine (PC) as PhL derives from its commercial availability and biorelevance.

Thus, the present work represents the following issues: (1) the spectral characterization of chosen push–pull dye molecules in organic solutions, (2) the modeling of the possible mechanisms of the temperature-induced spectral response of the dyes in organic media; (3) experimental evaluation of the structure requirements for efficient formation of dye-PC aggregates, (4) monitoring of the fluorescence changes under temperature variation within the so-called physiological range, (5) cytotoxicity and flow cytometry characterization of dye-PC bilayers, (6) intracellular localization of the dye-PC aggregates by fluorescent and confocal microscopy methods. The results will be correlated and discussed in order to highlight structure–property relationships forming the basis for the structural optimization of the systems in order to provide both internalization of the dye-PC bilayers in cells and high temperature sensitivity of their spectra.

2. Experimental section

2.1. Materials

6-Bromobenzo[*d*]thiazole, L-α-phosphatidylcholine destearoyl, DCM, tris(hydroxymethyl)aminomethane, Propidium Iodide, Rhodamine B and DMF were purchased from Acros or Aldrich.

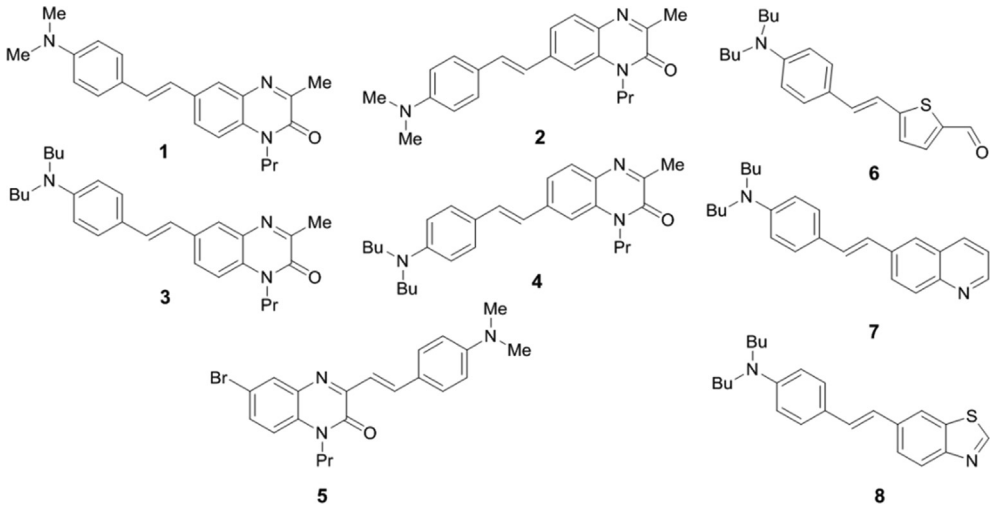

Scheme 1. Structures of dyes **1–8.**

2.2. Synthesis of the dyes

Dyes **1**–**6** were synthesized according to previously published procedures [29–32]. The synthesis of **7** and **8** and their characterization by ^{1}H NMR, IR and HRMS is described in details in SI.

2.3. Synthesis of the dye-PC aggregates and quantitative experimental evaluation of the dye:PC molar ratio.

The detailed descriptions of the modified thin-film hydration procedure and the measuring of the residual amounts of the dye after the hydration step can be found in SI.

2.4. Methods

The NMR, IR and MALDI spectra were registered on the equipment of Assigned Spectral-Analytical Center of FRC Kazan Scientific Center of RAS. NMR experiments were performed with Bruker AVANCE-400 (400 MHz for ^{1}H NMR, 100 MHz for ^{13}C NMR) spectrometers. Chemical shifts (δ in ppm) are referenced to the solvent. Infrared (IR) spectra were recorded on the Bruker Vector-22 FT IR spectrometer. The melting points of dyes **7** and **8** were determined by Melting Point Meter MF-MP-4.

Electronic absorption (UV–Vis) spectra were recorded at room temperature on a Perkin-Elmer Lambda 35 spectrometer with a scan speed of 480 nm/min, using a spectral width of 1 nm. All samples were prepared as solutions in dichloromethane with concentrations of $\sim 10^{-5}$ mol · L^{-1} and placed in 10 mm quartz cells.

The emission spectra were recorded on a fluorescence spectrophotometer Hitachi F-7100 (Japan) with stigmatic concave diffraction grating. Excitation of samples was performed at 350 nm and emission was detected at 400–700 nm.

The high resolution mass spectra(HRMS) of **7** and **8** were obtained on a Bruker Ultraflex III MALDI-TOF/TOF mass spectrometer in the reflectron mode. The device is equipped with a solid-state laser Nd:YAG laser (λ = 355 nm, repetition rate 100 Hz). Measurements were made in the range *m*/*z* 200–1000. A mixture of the sample (0.01 mg/mL, CH_3CN) and calibrant PEG-400 (1 mg/mL, CH_3CN) was prepared to determine the exact mass values. *para*-Nitroaniline (10 mg/mL, CH_3CN) was used as a matrix. Portions (0.5 μL) of the matrix solution and the analyzed mixture were sequentially applied to the target and evaporated. The metal target MTP AnchorChip™ was used. The specified composition allowed to provide the absolute error in determining the masses no more than 0.003 Da. The *m*/*z* values of monoisotopic ions are given in the descriptions. The data was obtained using the FlexControl program (Bruker Daltonik GmbH, Germany) and processed using the FlexAnalysis 3.0 program (Bruker Daltonik GmbH, Germany).

2.4.1. Quantum chemical computations

Free energies of implicitly solvated solute species were calculated with the recently developed CENSO protocol [33] for structure ensembles of non-rigid molecules. Therein, all structures of isolated conformers of the dyes under study (e.g., Figure S6) were optimized with the r^{2}SCAN-3c [34] composite density functional employing the direct COSMO-RS (DCOSMO-RS) [35] model, which enables geometry optimization in solution. The optimized geometries were further used for the single-point calculations of the electronic energies (*E*) by applying the PW6B95 [36]-D3 functional in combination with the quadruple-zeta def2-QZVP Ahlrich's basis set [37]. Herein "-D3" appended to the functional name means the D3 London dispersion correction in the Becke-Johnson sampling scheme [38,39]. Solvation contributions δG_{solv} to the free energy at 298.15 K were computed from the r^{2}SCAN-3c/DCOSMO-RS structures with the COSMO-RS method [40] based on BP86 [41,42] calculations with TZVP basis set [43]. The thermostatistical contribution to the free energy was computed by single-point hessian calculations [44] within the framework of the modified rigid-rotor-harmonic-oscillator statistical treatment (G_{mRRHO}) [45,46] at the level of semiempirical quantum chemical method GFN2-xTB [47] in combination with ALPB implicit solvation model [48]. The computed free energies in solution are then obtained by $G_{solution}$ = *E*(PW6B95-D3/def2-QZVP) + G_{mRRHO}(GFN2-xTB/ALPB) + δG_{solv}(COSMO-RS).

2.4.2. Cytotoxicity assay

Cytotoxic effects of the test compounds on human cancer and normal cells were estimated by means of the multifunctional Cytell Cell Imaging system (GE Health Care Life Science, Sweden) using the Cell Viability Bio App which precisely counts the number of cells and evaluates their viability from fluorescence intensity data. Two fluorescent dyes that selectively penetrate the cell membranes and fluoresce at different wavelengths were used in the experiments. A low-molecular-weight 4′,6-diamidin-2-phenylin dol dye (DAPI) is able to penetrate intact membranes of living cells and color nuclei in blue. High-molecular propidium iodide dye penetrates only dead cells with damaged membranes, staining them in yellow. As a result, living cells are painted in blue and dead cells are painted in yellow. DAPI and propidium iodide were purchased from Sigma. The M−Hela clone 11 human, epithelioid cervical carcinoma, strain of Hela, clone of M−Hela from the Type Culture Collection of the Institute of Cytology (Russian Academy of Sciences) and Chang liver cell line (Human liver cells) from N. F. Gamaleya Research Center of Epidemiology and Microbiology were used in the experiments. The cells were cultured in a standard Eagle's nutrient medium manufactured at the Chumakov Institute of Poliomyelitis and Virus Encephalitis (PanEco company) and supplemented with 10% fetal calf serum and 1% nonessential amino acids. The cells were plated into a 96-well plate (Eppendorf) at a concentration of 100,000 cells/mL, 150 μL of medium per well, and cultured in a CO_2 incubator at 37 °C. Twenty-four hours after seeding the cells into wells, test compounds were added at a preset dilution, 150 μL to each well. The dilutions of the compounds were prepared immediately in nutrient media. The experiments were repeated three times. Intact cells cultured in parallel with experimental cells were used as a control.

2.4.3. Cellular uptake study

M−HeLa cells in the amount of 1×10^5 cells / well in a final volume of 500 μL were sown in 24-well plates (Eppendorf). After 24-hour incubation, PC-**7** aggregates at a concentration of 7.5 μM were added to the wells and incubated for 24 h in a CO_2 incubator. Cellular uptake of test compounds was analyzed by flow cytometry (Guava easy Cyte 8HT, USA). Flow cytometry was used to set up statistics on the uptake of drug by cancer cells. Untreated cells were used as negative control.

2.4.4. Fluorescence microscopy

M−HeLa cells at 1×10^5 cells / well in a final volume of 2 ml were seeded into 6-well plates at the bottom of each well. After 24 h of incubation, solution of PC-**7** (7.5 μM) was added to the wells and cultured for 24 h in a CO_2 incubator. Then, M−HeLa cells were fixed and stained with DAPI (blue). The studies were carried out using a Nikon Eclipse Ci-S fluorescence microscope. (Nikon, Japan) at 1000x magnification.

2.4.5. Confocal laser microscopy

The control M−Hela cells and corresponding cells incubated with PC-**7** aggregates were visualized by CLMS on an inverted Carl Zeiss LSM 780 confocal laser-scanning microscope (CarlZeiss, Jena, Germany).

3. Results and discussion

3.1. Synthesis and spectral characterization of the dyes

To estimate possible influence of both electron-donor and electron-acceptor parts of dyes on their spectral behaviour as well as their interactions with PhL bilayers, a series of quinoxalinones (*Qons*) **1**–**5** with different position of donor dialkylaniline group relative to acceptor heterocyclic core has been complemented by dyes **6**–**8** with three different acceptor moieties (Scheme 1).

Dyes **1**–**6** were synthesized according to previously published procedures [29–32]. Both synthetic scheme (Scheme S1) and details of synthetic procedure for dyes **7** and **8** are represented in SI.

3.2. Temperature-induced spectral changes of the dyes in organic media

As shown elsewhere [29], dyes **1**–**5** demonstrate notable halochromism in the dichloromethane (DCM) solutions at room temperature, and being incorporated into PhL bilayers show spectral response to the pH change in water, that is caused by the protonation of the *Qons*.

As mentioned in the Introduction, the equilibrium between neutral and protonated forms of dyes in the acidified solutions should be influenced by temperature. This temperature dependence could be utilized for spectroscopic thermometry of biological environment provided that the bands of both forms are observed at rather neutral conditions. Among the studied dyes, **1** and **3** demonstrated both emission bands of comparable intensities at the lowest amounts of trifluoroacetic acid (TFA) compared to others (1:5 and 1:1 *Qon*:TFA ratios, respectively [29]). Previously reported ^{1}H NMR, UV–Vis spectral and quantum chemical computational analysis [29] highlight the protonation of the donor dialkylaniline group of dyes **1** and **3** in acidified DCM solutions as the reason for the strengthening of high-energy (HE) bands in their emission spectra. Thus, emission spectra of DCM solutions of chosen dyes with indicated amounts of TFA have been recorded in the temperature range from 10 to 39 °C (up to DCM boiling temperature).

Analysis of spectral response of acidified DCM solutions of **1** and **3** (Fig. 1) shows that the heating of the samples leads to shift of the equilibrium to the neutral species: increase of temperature causes the lowering of HE bands, associated with protonated forms and strengthening of low-energy (LE) bands, related to neutral forms. This, as well as the opposite cooling effect, shows that protonated forms of **1** and **3** are energetically more preferable than their neutral counterparts. Interestingly that besides the expected rearrangement of bands intensities, a blue shift of LE emission with the temperature increase is revealed.

To find out if the blue shift of the neutral form emission is related to the acid-base equilibrium or is it an immanent spectral feature of neutral dyes, the temperature dependence of emission spectra of neutral solutions of dyes **1**–**8** has been studied (Fig. 2). For all the compounds heating leads to blue shift of the emission band by 10–15 nm. One of the possible reasons for this effect may be thermal structural fluctuations producing non-planarity of the dye molecule and the concomitant disruption of π-conjugation between the heterocyclic moieties of the molecule. Interestingly that for compounds **1** – **4** this shift is accompanied by intensification of the corresponding band, whereas for dyes **5** – **8** increase of temperature leads to the quenching of the emission. For dyes **5**, **6**, **8** both wavelengths and intensities almost coincide for the same temperatures in the heating and cooling processes, while for the other dyes the process is not fully reversible (Fig. 2).

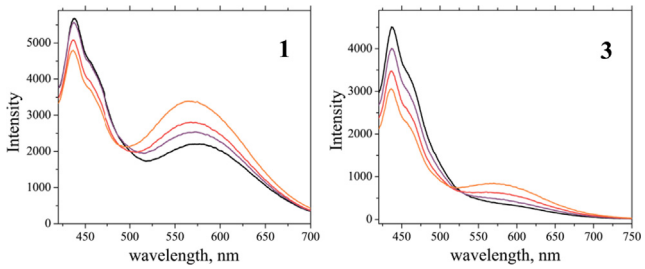

Fig. 1. Emission spectra of *Qons* **1** and **3**, recorded at 10 °C (black), 20 °C (purple), 30 °C (red) and 39 °C (orange).

Nevertheless, the temperature-dependent spectral behavior of the dyes in the neutral solutions provides promising basis for their biomedical applicability, since majority of biological liquids, including cell cytoplasm, are neutral with pH about 7.4. As shown elsewhere [29], the incorporation of the dyes into PC-based bilayers provides a facile route to convert the dyes to a water-soluble form.

3.3. Synthesis of dye-PC bilayers.

The abovementioned approach [29] was applied to the dyes shown in Scheme 1 for the formation of PC-dye mixed aggregates. The DLS measurements of the produced aggregates reveal their average size above 300 nm (Fig. S7). The optimal dye structures for the inclusion into the PC-based bilayers formed under the thin film hydration step (Fig. S5), for more details see the Experimental section) were revealed by the comparison of the experimentally measured molar PC:dye ratios for the different dyes. The results represented in Fig. 3 indicate the importance of the NBu_2 moieties versus NMe_2 ones for the more efficient incorporation of the dyes into the PC-bilayers: compare **3** vs **1**, and **4** vs **2.**

It is worth assuming that the formation of the mixed PC-dye bilayers is facilitated by an inclusion of the dyes into the hydrophobic layer of the bilayers, driven by the hydrophobicity of the dyes. Indeed, according to our quantum chemical computations of free energies in solution ($G_{solution}$) of conformational ensembles of molecules **1** and **3** by the recently developed CENSO protocol [33], the both species are more efficiently solvated by hexadecane than by water. Nevertheless, the difference between G_{water} and $G_{hexadecane}$ calculated for **3** (9.6 kcal mol^{-1}) essentially exceeds the difference of 6.2 kcal mol^{-1} computed for **1**, which suggests that a presence of the NBu_2 moiety should increase the fixation of **3** in the hydrophobic zone of PC bilayer relative to the case of molecule **1** containing NMe_2 moiety.

3.4. Temperature dependent emission of dye-PC aggregates

It is known that the arrangement of a dye within PhL bilayers dispersed in aqueous media strongly influences the dye fluorescence. In particular, the dye Prodan (N,N-Dimethyl-6-propionyl-2-naphthylamine) with low inclusion into hydrophobic lipid bilayer exhibit the fluorescence quenching accompanied by the red shift of the emission band in response to the temperature-induced phase transitions of the PhL bilayers producing a dislocation of Prodan from their hydrophobic core to polar periphery and bulk water [4]. Similar studies of another dyes included into PhL aggregates [3,5,6] also highlight increase in the polarity and hydration-induced quenching as the main reasons for the weakening of the dyes fluorescence. The temperature-induced fluorescent responses of the dyes within the PC-dye aggregates shown in Fig. 4 differ from the tendencies revealed in the aforesaid reports.

Monitoring of the emission spectra at different temperatures reveals a significant response to heating and cooling for dyes **3**, **4**

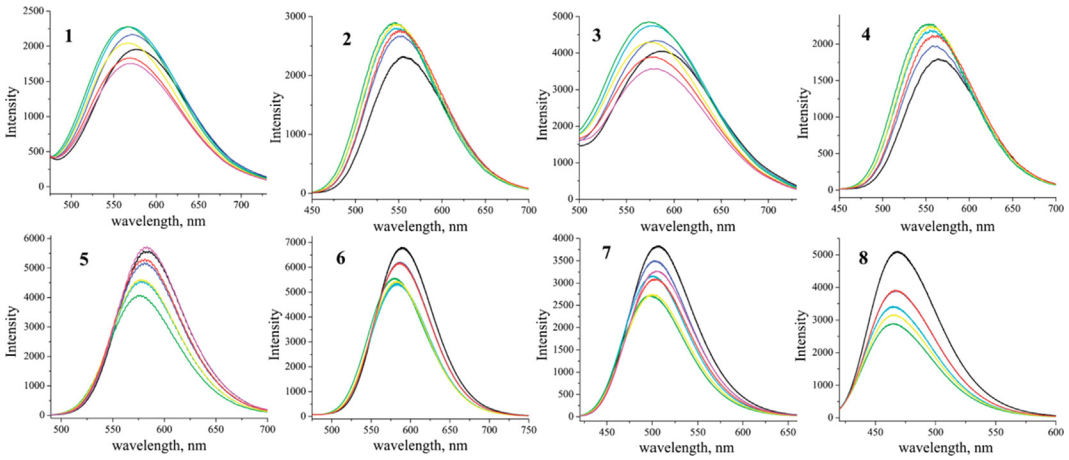

Fig. 2. Emission spectra of **1**–**8**, registered upon heating: at 10 °C (black), 20 °C (blue), 30 °C (light blue), 39 °C (green) and cooling: at 30 °C (yellow), 20 °C (red), 12 °C (magenta).

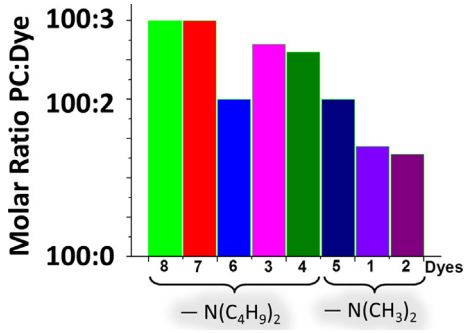

Fig. 3. The PC:dye ratios in the PC-dye aggregates represented for the dyes bearing $N(Bu)_2$ (**3**, **4**, **6**–**8**) and $N(Me)_2$ (**1**, **2**, **5**) moieties.

and **7** (Fig. 4), which is manifested by intensity changes in the range of 80–100% of the initial intensity. These temperature-induced intensity variations are smaller for fluorescence of PC aggregates with **1** (24%) and **6** (14%), whereas for **2, 5, 8** they do not exceed 4–6% of the initial intensity (Fig. S8). It is worth noting that the response on heating–cooling cycles was monitored at pH 7.4, while the insignificant changes in the emission (Fig. S8) are observed at pH within 5.0–6.0 (maximal allowable acidity for further bio-applications [6,49,50]). Thus, the temperature sensing, based on thermal control of acid-base equilibrium is not applicable for the water solutions. Nevertheless, the heating of the PC-dye aggregates, comprising **3**, **4** and **7** blue-shifts the emission bands similarly to the case of DCM solutions (vide supra). This similarity suggests that the same factors are responsible for qualitatively the same temperature dependence observed for the dyes in the organic solutions and in the PC matrix.

Nevertheless, in contrast to the solutions in DCM, the heating induces the insignificant changes for the dyes **1, 2, 5, 6, 8** incorporated into the PC-dye aggregates. Probably, this difference results from mutual compensation of two kinds of effects: (1) heating-induced blue shift and intensification of emission immanent for the dyes in organic medium (Fig. 2); and (2) the red-shifting and quenching of the fluorescence caused by a displacement of the dyes from the hydrophobic core of PC matrix to its polar periphery and/or bulk water. It should be noted that both the red shift of emission maximum and decrease of quantum yield induced by increasing polarity of solvents was, indeed, reported earlier for **1** and **3** [26]. Thus, only for the three dyes, **3**, **4** and **7**, in PC-dye

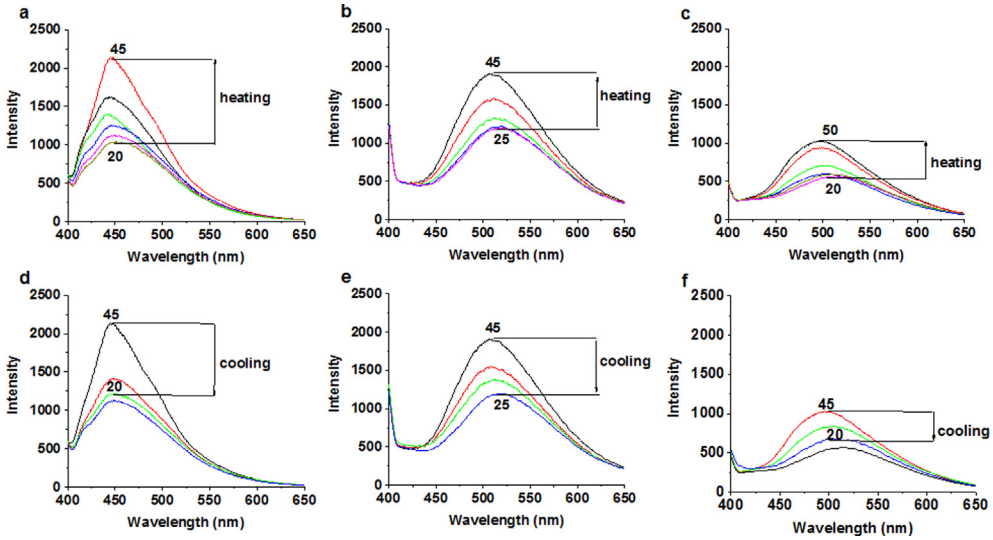

Fig. 4. Luminescence spectra of PC-Dye (0.5 mM PC, 0.015 mM dye, pH = 7.4) at heating and cooling respectively for: a,d – **7** (λ_{ex} = 390 nm); b,e – **3** (λ_{ex} = 370 nm); c,f – **4** (λ_{ex} = 415 nm).

aggregates the influence of the factor (1) is stronger than the impact of the factors (2).

The heating-induced emission enhancement is most pronounced for dyes **3** and **7**, which is the reason for further studies aimed at assessing the reproducibility of their emission in the heating–cooling cycles. The spectral data in Fig. 5 indicate the detectable irreversibility in the temperature-dependent fluorescence intensity of PC-**3,** while the fluorescence of PC-**7** exhibits greater recyclability within three heating–cooling cycles, followed by the detectable degradation under the further repeating of the heating–cooling cycles (Fig. 5). The well-known photochemical activity of dyes affected by solvent, temperature and oxygenation conditions [51] may be responsible for the irreversible fluorescence of PC-dye aggregates. It is worth assuming that heating of the PC-dye aggregates can enhance photo-induced transformations of the dye molecules, which are manifested in the irreversible spectral behavior of PC-**3** under the repeating of the heating–cooling cycles (Fig. 5 c, d), while the thermal stability of PC-**7** is sufficient within the three repeated cycles (Fig. 5 a, b). This suggests that the replacement of the quinoxalinone moiety in **3** by the heterocyclic substituent in **7** is a possible reason for the higher thermal stability of PC-**7** compared to PC-**3**. Moreover, the aforesaid structural difference can affect the localization of **3** and **7** within the hydrophobic and polar zones of PC-bilayers, which is another possible reason for the different stabilities of the dyes [12].

Thus, the temperature dependent spectral behavior of dye-PC aggregates is affected by the interference of the thermal structural fluctuations of the dyes with their displacement from the hydrophobic core of PC matrix to its polar periphery and/or bulk water, although a photochemical activity of the dyes somewhat restricts the reversibility of their spectral behavior under repeating of heating and cooling cycles. The stability of luminescence of PC-**7** is the greatest among the other aggregates (Fig. 5), which highlights PC-**7** as the leader for further cellular studies aimed at revealing their intracellular applicability.

3.5. Cytotoxicity and cellular uptake behavior of PC-7

Cellular uptake behavior of PC-**7** aggregates is a prerequisite for their usability in intracellular sensing. Commonly, a cytoplasmic entry of phospholipid-based aggregates undergoes through an interplay of several endocytosis mechanisms, including clathrin-mediated endocytosis and lipid fusion [49]. The fluorescence of PC-**7** aggregates provides an opportunity to monitor their cell internalization through flow cytometry, fluorescent and confocal microscopy methods. However, these studies should be preceded by cytotoxicity measurements. Thus, cell viabilities of M–HeLa and Chang Liver cell lines were evaluated after their 24 h incubation with PC-**7**. The quantitative analysis of the results indicates no significant cytotoxic effect on the cell samples incubated by PC-**7**, when the concentration of the dye varies within 2–15 μM, which amplifies that the IC_{50} values are above 15 μM (Table S1). This suggests the use of PC-**7** at the dye concentration below 15 μM for the imaging of the cells without significant suppressing of the cell viability. The flow cytometry data measured for M–HeLa cell samples incubated by PC-**7** aggregates (Fig. S9) reveal their cellular uptake at 7.5 μM of the dye, which results in efficient staining of the cell compartments as it is demonstrated by fluorescent microscopy image in Fig. S10. However, the fluorescent microscopy imaging is not enough to detail the intracellular localization of PC-**7** aggregates.

The confocal microscopy imaging of M–HeLa cell samples incubated by PC-**7** was performed to specify the localization of the dye within cell cytoplasm and nuclei. Therefore, the cell nuclei were additionally stained by red through the co-incubation with Propidium Iodide. The images at Fig. 6 indicate very poor if any colocal-

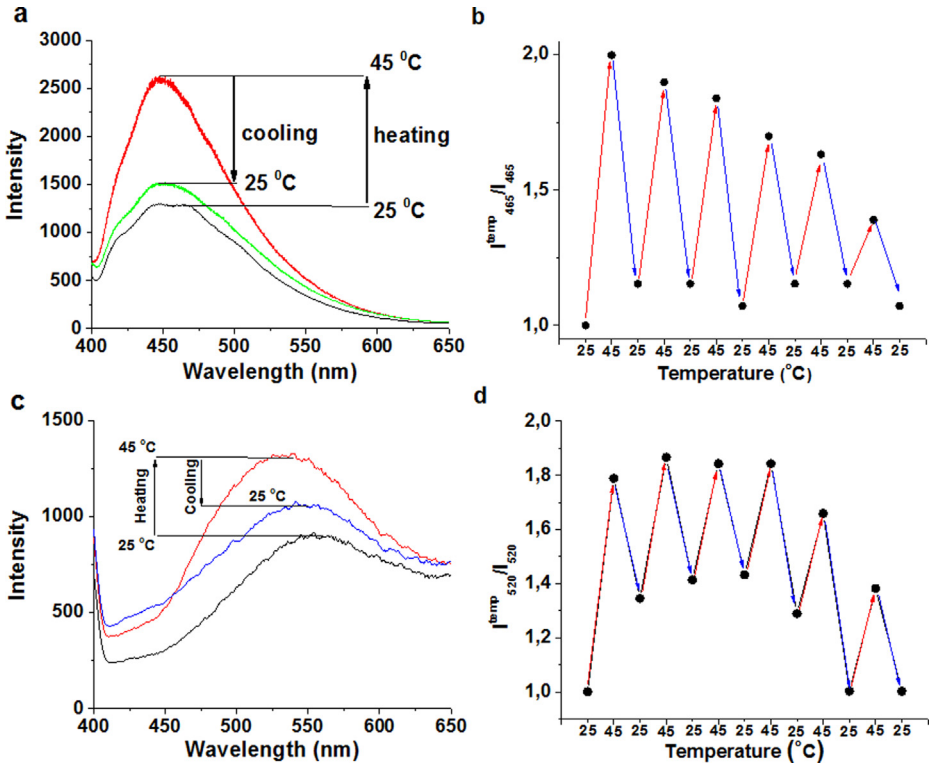

Fig. 5. Luminescence spectra of PC-**7** (a) (λ_{ex} = 390 nm) and PC-**3** (c) (λ_{ex} = 390 nm) under cyclical heating from 25 °C to 45 °C and cooling from 45 °C to 25 °C (pH = 7.4): b, d – I/I_0 (the luminescence intensity under cooling or heating normalized to the initial intensity) for PC-**7** (465 nm) and PC-**3** (520 nm) under the cyclical heating and cooling.

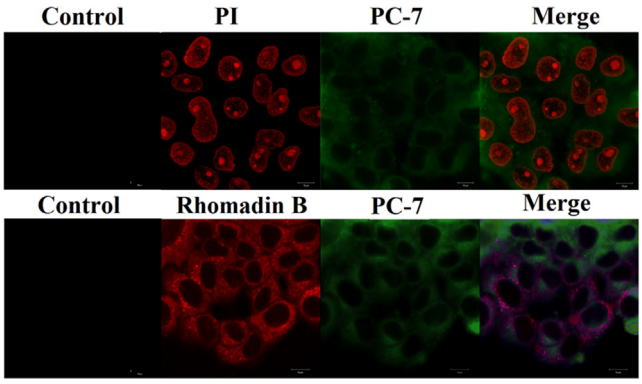

Fig. 6. Live imaging confocal microscopy (scale bar 10 μm) of M−HeLa cell samples incubated with PC-**7** (detectable interval 420–510 nm) and co-incubated by Propidium Iodide (detectable interval 566–716 nm) and Rhodamine B (detectable interval 548–703 nm), λ_{ex} = 405 nm.

ization of PC-**7** and Propidium Iodide in the cell nuclei. The staining by red of the cell cytoplasm through the co-incubation by Rhodamine B indicates the significant colocalization of the latter with the green emitting **7**, which highlights the applicability of PC-**7** as the cellular marker predominantly staining cell cytoplasm.

4. Conclusions

Summarizing, several dialkylaminostyrylhetarene dyes constructed from electron-rich and electron-deficient moieties connected *via* vinylene π-bridges are characterized as temperature-sensitive luminophores. Temperature-induced wavelength and intensity changes of dyes emission in neutral dichloromethane solutions make dyes a promising basis for the development of nanoparticles exhibiting thermal sensitivity in aqueous solutions at neutral pH of biological liquids. Hydrophobicity-driven incorporation of the water insoluble dyes into L-α-phosphatidylcholine(PC)-based bilayers allows to obtain water dispersible dye-PC aggregates, and to follow their emission in the aqueous solutions. Structure of the dyes has strong impact on the efficacy of the dyes incorporation into the PC-based bilayers, temperature sensitivity of emission of the dye-PC aggregates and its reversibility under the heating/cooling cycles. This enables structural optimization of the dyes in order to obtain the dye-PC species demonstrating maximal temperature dependence and reversibility of their luminescence in aqueous solutions. The low cytotoxicity of the selected leader among the dye-PC aggregates was exemplified for M−HeLa and Chang Liver cell lines. The efficient staining of cell cytoplasm by the dye-PC luminophores opens further opportunities for biosensing applications.

CRediT authorship contribution statement

B.S. Akhmadeev: Formal analysis, Investigation, Data curation, Writing – original draft, Writing – review & editing, Visualization. **T.P. Gerasimova:** Methodology, Formal analysis, Investigation, Writing – original draft. **A.R. Gilfanova:** Formal analysis. **S.A. Katsyuba:** Conceptualization, Methodology, Validation, Formal analysis, Writing – original draft, Writing – review & editing. **L.N. Islamova:** Formal analysis, Investigation. **G.M. Fazleeva:** Formal analysis, Investigation. **A.A. Kalinin:** Conceptualization, Investigation, Methodology, Validation, Formal analysis, Data curation. **A.G. Daminova:** Formal analysis, Investigation. **S.V. Fedosimova:** Formal analysis, Investigation. **S.K. Amerhanova:** Formal analysis, Investigation. **A.D. Voloshina:** Formal analysis, Investigation. **E.G. Tanysheva:** Formal analysis, Investigation. **O.G. Sinyashin:** Conceptualization, Supervision, Project administration, Funding acquisition. **A.R. Mustafina:** Conceptualization, Methodology, Validation, Formal analysis, Data curation, Writing – original draft, Writing – review & editing.

Declaration of Competing Interest

The authors declare that they have no known competing financial interests or personal relationships that could have appeared to influence the work reported in this paper.

Acknowledgements

This work is supported by the Russian Science Foundation under grant 19-13-00163. Authors gratefully acknowledge to Assigned Spectral-Analytical Center of FRC Kazan Scientific Center of RAS for providing necessary facilities to carry out physical-chemical measurements. The authors are grateful to Prof. S. Grimme for permission to use his program CENSO [33] and computational facilities of Mulliken Center for Theoretical Chemistry (Institut für Physikalische und Theoretische Chemie der Universität Bonn), as well as for his valuable advice.

Appendix A. Supplementary material

Supplementary data to this article can be found online at https://doi.org/10.1016/j.saa.2021.120647.

References

[1] K. McNamara, T. Nguyen, G. Dumitrascu, J. Ji, N. Rosenzweig, Z. Rosenzweig, Synthesis, characterization, and fpplication of fluorescence censing lipobeads for Intracellular pH measurements, Anal. Chem. 73 (2001) 3240–3246, https://doi.org/10.1021/ac0102314.
[2] B. Villeponteau, J. Brawley, H.G. Martinson, Nucleosome spacing is compressed in active chromatin domains of chick erythroid cells, Biochemistry 31 (5) (1992) 1554–1563, https://doi.org/10.1021/bi00120a037.
[3] C.A. Gobrogge, V.A. Kong, R.A. Walker, Temperature dependent solvation and Partitioning of coumarin 152 in phospholipid membranes, J. Phys. Chem. B 120 (2015) 1805–1812, https://doi.org/10.1021/acs.jpcb.5b0950.
[4] M. Goto, A. Wilk, A. Kazama, S. Chodankar, J. Kohlbrecher, H. Matsuki, Chain elongation of diacylphosphatidylcholine induces fully bilayer interdigitation under atmospheric pressure, Colloids Surf. B 84 (1) (2011) 44–48, https://doi.org/10.1016/j.colsurfb.2010.12.010.
[5] K. Ng, M. Shakiba, E. Huynh, R.A. Weersink, A. Roxin, BC Wilson BC, Zheng G, Stimuli-responsive photoacoustic nanoswitch for in vivo sensing, ACS Nano 8 (2014) 8363–8373, https://doi.org/10.1021/nn502858b.
[6] V. Coste, N. Puff, D. Lockau, P.J. Quinn, M.I. Angelova, Raft-like domain formation in large unilamellar vesicles probed by the fluorescent phospholipid analogue, C12NBD-PC, Biochim. Biophys. Acta 1758 (4) (2006) 460–467, https://doi.org/10.1016/j.bbamem.2006.03.003.
[7] O.A. Kucherak, S. Oncul, Z. Darwich, D.A. Yushchenko, Y. Arntz, P. Didier, I. Mely, A.S. Klymchenko, Switchable nile red-based probe for cholesterol and lipid order at the outer leaflet of biomembranes, J. Am. Chem. Soc. 132 (13) (2010) 4907–4916, https://doi.org/10.1021/ja100351w.
[8] A. Kyrychenko, F. Wu, R.P. Thummel, J. Waluk, A.S. Ladokhin, Partitioning and localization of environment-sensitive 2-(2′-Pyridyl)- and 2-(2′-Pyrimidyl)-Indoles in lipid membranes: A joint refinement using fluorescence measurements and molecular dynamics simulations, J. Phys. Chem. B 114 (42) (2010) 13574–13584, https://doi.org/10.1021/jp106981c.
[9] V.M. Trusova, E. Kirilova, I. Kalnina, G. Kirilov, O.A. Zhytniakivska, P.V. Fedorov, G.P. Gorbenko, Novel benzanthrone aminoderivatives for membrane studies, J. Fluoresc. 22 (3) (2012) 953–959, https://doi.org/10.1007/s10895-011-1035-8.
[10] P. Franken Dick, F.L. Coelho, F.S. Rodembusch, L.F. Campo, Amphiphilic ESIPT benzoxazole derivatives as prospective fluorescent membrane probes, Tetrahedron Lett. 55 (19) (2014) 3024–3029, https://doi.org/10.1016/j.tetlet.2014.03.103.
[11] M. Sánchez, F.J. Aranda, J.A. Teruel, A. Ortiz, New pH-sensitive liposomes containing phosphatidylethanolamine and a bacterial dirhamnolipid, Chem. Phys. Lipids 164 (1) (2011) 16–23, https://doi.org/10.1016/j.chemphyslip.2010.09.008.
[12] J. Cauzzo, M. Nystad, A.M. Holseter, P. Basnet, N. Skalko-Basnet, Following the fate of dye-containing liposomes in vitro, Int. J. Mol. Sci. 21 (14) (2020) 4847, https://doi.org/10.3390/ijms21144847.
[13] M. Breton, G. Prével, J.-F. Audibert, R. Pansu, P. Tauc, B.L. Pioufle, O. Français, J. Fresnais, J.-F. Berret, E. Ishow, Solvatochromic dissociation of non-covalent

fluorescent organic nanoparticles upon cell internalization, Phys. Chem. Chem. Phys. 13 (29) (2011) 13268, https://doi.org/10.1039/c1cp20877b.
[14] W.-H. Li, Probes for monitoring regulated exocytosis, Cell Calcium 64 (2017) 65–71.
[15] Y. Wu, F.L. Yeh, F. Mao, E.R. Chapman, Biophysical characterization of styryl dye-membrane interactions, Biophys. J. 97 (1) (2009) 101–109, https://doi.org/10.1016/j.bpj.2009.04.028.
[16] A. Zweifach, FM1-43 reports plasma membrane phospholipid scrambling in T-lymphocytes, Biophys. J. 97 (2009) 101–109, https://doi.org/10.1016/j.bpj.2009.04.028.
[17] M.A. Gaffield, W.J. Betz, Imaging synaptic vesicle exocytosis and endocytosis with FM dyes / Nat Protoc 1 (6) (2006) 2916–2921, https://doi.org/10.1038/nprot.2006.476.
[18] C. Guatimosim, M.A. Romano-Silva, M.V. Gomez, M.A.M. Prado, Use of fluorescent probes to follow membrane traffic in nerve terminals, Braz. J. Med. Biol. Res. 31 (11) (1998) 1491–1500, https://doi.org/10.1590/S0100-879X1998001100018.
[19] Z. Zhang, W. Cao, H. Jin, J. Lovell, M.i. Yang, L. Ding, J. Chen, I. Corbin, Q. Luo, G. Zheng, Biomimetic nanocarrier for direct cytosolic drug delivery, Angew. Chem. Int. Ed. 48 (48) (2009) 9171–9175, https://doi.org/10.1002/anie.200903112.
[20] W.D. Niles, A.B. Malik, Endocytosis and exocytosis events regulate vesicle traffic in endothelial cells, J. Membr. Biol. 167 (1) (1999) 85–101, https://doi.org/10.1007/s002329900474.
[21] S. Sun, P. Li, S. Liang, Z. Yang, Diversified copper sulfide ($Cu_{2-x}S$) micro-/nanostructures: A comprehensive review on synthesis, modifications and applications, Nanoscale 9 (32) (2017) 11357–11404, https://doi.org/10.1039/C7NR03828C.
[22] A.E. Deatsch, B.A. Evans, Heating efficiency in magnetic nanoparticle hyperthermia, J. Magn. Magn. Mater. 354 (2014) 163–172, https://doi.org/10.1016/j.jmmm.2013.11.006.
[23] I.E. Kolesnikov, M.A. Kurochkin, I.N. Meshkov, R.A. Akasov, A.A. Kalinichev, E.Y. Kolesnikov, Y.G. Gorbunova, E. Lähderanta, Water-soluble multimode fluorescent thermometers based on porphyrins photosensitizers, Mater. Des. 203 (2021) 109613, https://doi.org/10.1016/j.matdes.2021.109613.
[24] A.R. Mukhametshina, A.R. Mustafina, N.A. Davydov, I.R. Nizameev, M.K. Kadirov, V.V. Gorbatchuk, A.I. Konovalov, The energy transfer based fluorescent approach to detect the formation of silica supported phosphatidylcholine and phosphatidylserine containing bilayers, Colloids Surf. B 115 (2014) 93–99, https://doi.org/10.1016/j.colsurfb.2013.11.035.
[25] R. Jelinek, S. Kolusheva, Membrane Interactions of Host-defense Peptides Studied in Model Systems, Curr. Protein Pept. Sci. 6 (2005) 103–114, https://doi.org/10.2174/1389203053027511.
[26] T.I. Burganov, S.A. Katsyuba, S.M. Sharipova, A.A. Kalinin, A. Monari, X. Assfeld, Novel quinoxalinone-based push-pull chromophores with highly sensitive emission and absorption properties towards small structural modifications, Phys. Chem. Chem. Phys. 20 (33) (2018) 21515–21527, https://doi.org/10.1039/C8CP03780A.
[27] Y.H. Budnikova, Y.B. Dudkina, A.A. Kalinin, M.Y. Balakina, Considerations on electrochemical behavior of NLO chromophores: Relation of redox properties and NLO activity, Electrochimica. Acta 368 (2021) 137578, https://doi.org/10.1016/j.electacta.2020.137578.
[28] S. Bijesh, R. Misra, Triphenylamine Functionalized unsymmetrical quinoxalines, Asian J. Org. Chem. 7 (9) (2018) 1882–1892, https://doi.org/10.1002/ajoc.201800384.
[29] T.P. Gerasimova, T.I. Burganov, S.A. Katsyuba, A.A. Kalinin, L.N. Islamova, G.M. Fazleeva, B.S. Ahmadeev, A.R. Mustafina, A. Monari, X. Assfeld, O.G. Sinyashin, Halochromic luminescent quinoxalinones as a basis for pH-sensing in organic and aqueous solutions, Dyes Pigments 186 (2021) 108958, https://doi.org/10.1016/j.dyepig.2020.108958.
[30] S.M. Sharipova, A.A. Gilmutdinova, D.B. Krivolapov, Z.R. Khisametdinova, O.N. Kataeva, A.A. Kalinin, Synthesis of isomeric (E)-[4-(dimethylamino)phenyl]-vinylquinoxalines – precursors for a new class of nonlinear optical chromophores, Chem. Heterocycl. Compd. 53 (2017) 504–510, https://doi.org/10.1007/s10593-017-2084-y.
[31] O.D. Fominykh, A.A. Kalinin, S.M. Sharipova, A.V. Sharipova, T.I. Burganov, M.A. Smirnov, T.A. Vakhonina, A.I. Levitskaya, A.A. Kadyrova, N.V. Ivanova, A.R. Khamatgalimov, I.R. Nizameev, S.A. Katsyuba, M.Y. Balakina, Composite materials containing chromophores with 3,7(di)vinylquinoxalinone π-electron bridge doped into PMMA: Atomistic modeling and measurements of quadratic nonlinear optical activity, Dyes Pigments 158 (2018) 131–141, https://doi.org/10.1016/j.dyepig.2018.05.033.
[32] M.J. Patrick, L.A. Ernst, A.S. Waggoner, D. Thai, D. Tai, G. Salama, Enhanced aqueous solubility of long wavelength voltage-sensitive dyes by covalent attachment of polyethylene glycol, Org. Biomol. Chem. 5 (2007) 3347–3353, https://doi.org/10.1039/b711438a.
[33] S. Grimme, F. Bohle, A. Hansen, P. Pracht, S. Spicher, M. Stahn, Efficient quantum chemical calculation of structure ensembles and free energies for nonrigid molecules, J. Phys. Chem. A 125 (19) (2021) 4039–4054, https://doi.org/10.1021/acs.jpca.1c00971.
[34] S. Grimme, A. Hansen, S. Ehlert, J.-M. Mewes, r^2SCAN-3c: A "Swiss army knife" composite electronic-structure method, J. Chem. Phys. 154 (6) (2021) 064103, https://doi.org/10.1063/5.0040021.
[35] A. Klamt, M. Diedenhofen, Calculation of solvation free energies with DCOSMO-RS, *J.* Phys. Chem. A 119 (2015) 5439–5445, https://doi.org/10.1021/jp511158y.
[36] Y. Zhao, D.G. Truhlar, Design of density functionals that are broadly accurate for thermochemistry, thermochemical kinetics, and nonbonded interactions, J. Phys. Chem. A 109 (25) (2005) 5656–5667, https://doi.org/10.1021/jp050536c.
[37] F. Weigend, F. Furche, R. Ahlrichs, Gaussian basis sets of quadruple zeta valence quality for atoms H-Kr, J. Chem. Phys. 119 (24) (2003) 12753–12762.
[38] S. Grimme, J. Antony, S. Ehrlich, H. Krieg, A consistent and accurate ab initio parametrization of density functional dispersion correction (DFT-D) for the 94 elements H-Pu, J. Chem. Phys. 132 (2010) 154104–154119, https://doi.org/10.1063/1.3382344.
[39] S. Grimme, S. Ehrlich, L. Goerigk, Effect of the damping function in dispersion corrected density functional theory, J. Comp. Chem. 32 (7) (2011) 1456–1465, https://doi.org/10.1002/jcc.21759.
[40] F. Eckert, A. Klamt, Fast solvent screening via quantum chemistry: COSMO-RS Approach, AIChe*E* J. 48 (2) (2002) 369–385, https://doi.org/10.1002/aic.690480220.
[41] A.D. Becke, Density-functional exchange-energy approximation with correct asymptotic behavior, Phys. Rev. A 38 (6) (1988) 3098–3100, https://doi.org/10.1103/PhysRevA.38.3098.
[42] J.P. Perdew, Density-functional approximation for the correlation energy of the inhomogeneous electron gas, Phys. Rev. B 33 (12) (1986) 8822–8824, https://doi.org/10.1103/PhysRevB.33.8822.
[43] A. Schäfer, C. Huber, R. Ahlrichs, Fully optimized contracted Gaussian basis sets of triple zeta valence quality for atoms Li to Kr, J. Chem. Phys. 100 (8) (1994) 5829–5835, https://doi.org/10.1063/1.467146.
[44] S. Spicher, S. Grimme, Single-Point Hessian calculations for improved vibrational frequencies and rigid-rotor-harmonic-oscillator thermodynamics, J. Chem. Theory Comput. 17 (3) (2021) 1701–1714, https://doi.org/10.1021/acs.jctc.0c01306.
[45] S. Grimme, Supramolecular binding thermodynamics by dispersion-corrected density functional theory, Chem. Eur. J. 18 (32) (2012) 9955–9964, https://doi.org/10.1002/chem.201200497.
[46] S. Spicher, S. Grimme, Efficient computation of free energy contributions for association reactions of large molecules, J. Phys.Chem Lett 11 (16) (2020) 6606–6611, https://doi.org/10.1021/acs.jpclett.0c01930.
[47] C. Bannwarth, S. Ehlert, S. Grimme, GFN2-xTB – An accurate and broadly parametrized self-consistent tight-Binding quantum chemical method with multipole electrostatics and density-dependent dispersion contributions, J. Chem. Theory Comput. 15 (3) (2019) 1652–1671, https://doi.org/10.1021/acs.jctc.8b01176.
[48] S. Ehlert, M. Stahn, S. Spicher, S. Grimme, Robust and efficient implicit solvation model for fast semiempirical methods, J. Chem. Theory Comput. 17 (7) (2021) 4250–4261, https://doi.org/10.1021/acs.jctc.1c00471.
[49] T. Bus, A. Traeger, U.S. Schubert, The great escape: How cationic polyplexes overcome the endosomal barrier, J. Mater. Chem. B 6 (43) (2018) 6904–6918, https://doi.org/10.1039/C8TB00967H.
[50] N.D. Donahue, H. Acar, S. Wilhelm, Concepts of nanoparticle cellular uptake, intracellular trafficking, and kinetics in nanomedicine, Adv. Drug Deliv. Rev. 143 (2019) 68–96, https://doi.org/10.1016/j.addr.2019.04.008.
[51] A.P. Demchenko, Photobleaching of organic fluorophores: quantitative characterization, mechanisms, protection Methods, ApplFluoresc 8 (2) (2020) 022001, https://doi.org/10.1088/2050-6120/ab7365.